Membrane contact sites regulate vacuolar fission via sphingolipid metabolism

Kazuki Hanaoka[1,†], Kensuke Nishikawa[1,†], Atsuko Ikeda[1,†], Philipp Schlarmann[1], Sayumi Yamashita[2], Aya Nakaji[2], Sotaro Fujii[1] and Kouichi Funato[1,2*]

[1]Graduate School of Integrated Sciences for Life, Hiroshima University, Kagamiyama 1-4-4, Higashi-Hiroshima 739-8528, Japan.

[2]School of Applied Biological Science, Hiroshima University, Kagamiyama 1-4-4, Higashi-Hiroshima 739-8528, Japan.

[†]These authors contributed equally to this work

* Corresponding author; Kouichi Funato

Email: kfunato@hiroshima-u.ac.jp

Abstract

Membrane contact sites (MCSs) are junctures that perform important roles including coordinating lipid metabolism. Previous studies have indicated that vacuolar fission/fusion processes are coupled with modifications in the membrane lipid composition. However, it has been still unclear whether MCS-mediated lipid metabolism controls the vacuolar morphology. Here we report that deletion of tricalbins (Tcb1, Tcb2, Tcb3), tethering proteins at endoplasmic reticulum (ER)-plasma membrane (PM) and ER-Golgi contact sites, alters fusion/fission dynamics and causes vacuolar fragmentation in the yeast *Saccharomyces cerevisiae*. In addition, we show that the sphingolipid precursor phytosphingosine accumulates in tricalbin-deleted cells, triggering the vacuolar division. Detachment of the nucleus vacuole junction (NVJ), an important contact site between the vacuole and the perinuclear ER, restored vacuolar morphology in both cells subjected to high exogenous phytosphingosine and Tcb3-deleted cells, supporting that phytosphingosine transport across the NVJ induces vacuole division. Thus, our results suggest that vacuolar morphology is maintained by MCSs through the metabolism of sphingolipids.

Introduction

Cellular organelles are formed by membranes with unique lipid compositions, morphology, and functions. The vacuole of budding yeast is an organelle that shares many similarities with mammalian lysosomes and plant vacuoles. Vacuoles possess degradative and storage capacities, and are essential for maintaining cellular homeostasis, including maintaining pH or ion homeostasis, cellular detoxification, and responses to osmotic shock and nutrient environments. Vacuoles are liable to change their morphology (size, volume, and number) through cycles of fusion and fission, to adapt to the intracellular and extracellular environments or upon vacuole inheritance to daughter cells. The steady-state morphology of the vacuole is maintained by a balance of constitutive vacuolar fusion and fission processes [1] [2].

The homotypic vacuolar membrane fusion process occurs in four stages: priming, tethering, docking and fusion [3] [4] [5] [6]. Each stage is defined as follows. “Priming” In the priming reaction, inactive fusion factors that are still assembled from previous fusion events are recycled. The yeast N-ethylmaleimide-sensitive factor (NSF), Sec18p, is activated by ATP and releases the NSF attachment protein (SNAP), Sec17p, from the protease complex, thereby activating the SNAP receptor (SNARE) molecule [3] [4] [7]. “Tethering” The HOPS/Class C Vps complex and the Rab-GTPase Ypt7p mediate the reversible contact of opposing vacuoles [4] [8]. “Docking” The coupling of three Q-SNAREs (Vam3p, Vam7p, and Vti1p) with an opposing R-SNARE (Nyv1p) to form a trans-SNARE complex between the two corresponding vacuoles. “Fusion” The final stage in which the lipid bilayer fuses and the contents of the lumen are mixed [5] [7]. For stable vacuolar fusion, several factors are required such as vacuolar acidification by V-ATPase proton pump activity [1] [9] [10] [11], ions [12] and ion transporters [13].

Furthermore, vacuolar fission is required for proper vacuolar inheritance during mitosis and acute response to osmotic shock in yeast, however the molecular mechanism of fission is not fully understood, and limited knowledge is available. Vacuolar fission is performed in two steps that require proteins and lipids [14]. The first step is the contraction and invagination of the vacuolar membrane through the involvement of Vps1p, a dynamin-like GTPase [15] and V-ATPase, which drives the proton gradient [1]. Next, vacuolar fission is promoted by Vac14p, Vac7p, and Fab1p [16], which are required for the generation of PtdIns[3,5]P2, and Atg18p, an effector of Fab1p and a sensor of PtdIns[3,5]P2 levels [17] [18]. Recently, it has also been shown that vacuolar fission is associated with nutrient status and responds to ER stress via TORC1 targets [19] [20]. Moreover, it has been proposed that vacuolar fusion and fission dynamics are regulated by the Yck3p-Env7p kinase cascade, which maintains an equilibrium between fusion and fission activities [21].

Organelles construct a dynamic network by associating with each other through membrane-contact sites (MCSs), which play an important role in lipid transport and metabolism

65 [22] [23]. Lipids (phosphatidic acid (PA), diacylglycerol, ergosterol, phosphatidylinositol (PtdIns)
66 phosphate (PtdInsP)) and lipid raft domains have been shown to be important as fusion and fission
67 effectors and discussed in a variety of recent reviews [2] [17] [24] [25] [26] [27]. However, it remains
68 unclear if MCS-mediated lipid metabolism controls the morphology of the vacuole. Vacuoles have
69 contact sites with other organelles. The MCS where the nuclear ER meets the vacuole is called the
70 nucleus-vacuole junction (NVJ), and the ER-localized Nvj1p and vacuole-membrane-localized
71 Vac8p act as tethers to form the NVJ [28]. Vacuoles also form MCS with mitochondria called
72 vacuole and mitochondria patches (vCLAMP). vCLAMP is mediated by the soluble (cytosol-
73 localized) HOPS complex subunit Vps39p, the vacuole-localized small Rab-GTPase Ypt7p, and by
74 an unknown mitochondrial factor [29] [30]. The translocase of the mitochondrial outer membrane
75 (TOM) subunit Tom40p has been identified as a direct binding partner of Vps39p, suggesting a
76 mechanism for the formation of vCLAMP by the Ypt7p-Vps39p-Tom40p tether [31]. Although it has
77 been suggested that MCSs with vacuoles are involved in the transport of lipids such as sterols and
78 precursors of sphingolipids that are involved in vacuolar morphology [32] [33] [34] [35], the roles of
79 those MCSs-mediated lipid metabolisms in the regulation of vacuole morphology are not
80 understood.
81 In this study, we found that tether proteins of MCS formation are involved in the regulation
82 of vacuolar morphology. We show that the deletion of tricalbins, tethers of the MCS between the
83 ER and the plasma membrane (PM) [36] and between the ER and the Golgi apparatus [37], affects
84 vacuolar division. Phytosphingosine, a precursor of ceramide, accumulated in the tricalbin-deleted
85 strain and was revealed as the underlying cause that triggers vacuolar fission. Moreover, deletion
86 of key tethering proteins at the NVJ recovered vacuolar morphology of cells subjected to high
87 exogenous phytosphingosine and tricalbin-deleted cells, indicating that the NVJ is required for
88 phytosphingosine-induced vacuolar fission. In summary, we propose that vacuolar morphology is
89 regulated by MCSs through regulation of sphingolipid metabolic pathways.
90

Results

Deletion of tricalbins causes vacuole fragmentation

Tricalbins (Tcb1p, Tcb2p, and Tcb3p) are ER membrane tethering proteins that connect the cortical ER (cER) with the PM [38], and contribute to PI4P turnover [36], sterol flux and transport [39] and maintain other lipid homeostasis [40]. It is also suggested that tricalbins create ER membrane curvature to maintain PM integrity [41] [42]. Tricalbins also localize to the ER-Golgi contacts and are responsible for the non-vesicular transport of ceramide from ER to Golgi apparatus [37]. However, their role in other organelle morphology and function remains unknown. Interestingly, the *NVJ1* gene, which encodes a major component of the NVJ, showed a negative synthetic interaction with the absence of all three tricalbins (*tcb1*Δ*2*Δ*3*Δ) [41]. Moreover, HOPS subunit Vam6p and Rab-GTPase Ypt7p, which are both involved in vacuolar fusion, also showed negative synthetic interaction with *tcb1*Δ*2*Δ*3*Δ [41]. Based on the findings, we assumed that tricalbins may be involved in the regulation of vacuolar morphology or function linked with the NVJ. To investigate the role of tricalbins in vacuole morphology, we analyzed the number of vacuoles per cell by a fluorescent probe FM4-64 that selectively stains yeast vacuolar membranes. We observed that compared to wild type cells, the *tcb1*Δ*2*Δ*3*Δ strain showed a phenotype characterized by a decreased percentage of cells with one vacuole and an increased percentage of cells with two or more vacuoles (Fig 1A). We refer to this phenotype as vacuolar fragmentation. In addition, analysis with single- and double deletion strains revealed that single deletion of *TCB1* or *TCB3* already exhibited strong vacuole fragmentation (Fig 1B). These results indicate that tricalbins are important to maintain vacuole morphology.

We next examined whether deletion of tricalbins affects vacuolar acidification. As homotypic vacuole-vacuole membrane fusion requires the vacuolar H^+-ATPase (V-ATPase) [11] [43] [44], tricalbins could be indirectly involved in maintaining vacuole morphology through V-ATPase. Therefore, we addressed whether tricalbin mutant strains could grow in alkaline media, because V-ATPase–deficient mutants can grow in acidic media but fail to grow in alkaline media [43]. As a negative control, we used *vma3*Δ mutant cells in which one of the V0 subunits of V-ATPase had been deleted. The *vma3*Δ mutant cells grew in acidic medium (pH 5.0), but failed to grow in alkaline medium (pH 7.5) (Fig S1A). In contrast, all tricalbin mutant strains grew like wild type in both conditions, suggesting that the V-ATPase in these mutants remains functionally normal. Thus, these results suggest that vacuole fragmentation caused by tricalbin deletion is not due to a loss of function of V-ATPase.

Furthermore, we investigated the effects of tricalbin deletion on delivery of a vacuolar protease, carboxypeptidase S (Cps1p) that is sorted into the vacuole lumen upon endosome–vacuole fusion. Deletion of HOPS complex components that mediate endosome–vacuole fusion

127 results in vacuole fragmentation [45]. To test the possibility that vacuole fragmentation in tricalbin
128 mutant cells is caused by a defect of endosome–vacuole fusion, we analyzed the localization of
129 GFP-Cps1p in tricalbin mutant cells. In both of WT and *tcb3*Δ cells, GFP-Cps1p was observed in
130 the vacuole lumen (Fig S1B), suggesting that the tricalbin mutant exhibits a normal delivery of
131 vacuolar proteins via endosomes to the vacuole. In addition, the fact that tricalbin deletion does not
132 affect the maturation of CPY, a vacuolar hydrolase carboxypeptidase Y [37], indicates that the
133 vacuolar degradation ability as well as protein delivery to the vacuole is normal. Taken together,
134 tricalbins are required for maintaining vacuole morphology, but not due to an indirect action through
135 vacuolar acidification or endosome-vacuole fusion.
136
137 **Tricalbins negatively regulate vacuole fission in a parallel pathway with TORC1**
138 The number and size of vacuoles within a cell are regulated by coordinated cycles of
139 vacuolar fission and fusion. To address whether vacuole fragmentation in the tricalbin mutant is
140 caused by facilitation of vacuole fission or an impaired homotypic vacuole fusion, we examined the
141 effect of hypotonic stress on vacuole fragmentation in *tcb1*Δ*2*Δ*3*Δ mutant cells, because low-
142 osmotic stimuli such as water promote homotypic vacuole fusion to maintain cytoplasmic osmolarity
143 [46]. We observed that addition of water to *tcb1*Δ*2*Δ*3*Δ cells partially restored vacuole
144 fragmentation, suggesting that vacuolar fusion machinery is functional in *tcb1*Δ*2*Δ*3*Δ cells (Fig 1C).
145 This result suggests that loss of tricalbins alters fusion-fission dynamics by primarily affecting the
146 fission machinery rather than fusion.
147 As the target of rapamycin complex 1 (TORC1) is a positive regulator of vacuole fission in
148 response to hyperosmotic shock and ER stress [19] [20], we next examined if rapamycin, which is
149 an inhibitor of TORC1, affects the vacuole fragmentation in *tcb1*Δ*2*Δ*3*Δ cells. As shown in Figure
150 1C, we observed that the vacuole fragmentation in *tcb1*Δ*2*Δ*3*Δ cells was suppressed by rapamycin,
151 suggesting that TORC1 may be required for tricalbin deletion-induced vacuolar fragmentation. We
152 attempted to characterize further the relationship between tricalbin and TORC1, and showed that
153 *tcb1*Δ*2*Δ*3*Δ cells had no significant effect on phosphorylation levels of Sch9p, a major downstream
154 effector of TORC1 (Fig 1D). These results suggest that deletion of tricalbins does not activate
155 TORC1. Therefore, we conclude that tricalbins and TORC1 act in parallel and opposite ways to
156 regulate vacuole fission (Fig 1E).
157
158 **The TM domain of Tcb3 contributes to mediating protein interactions between the tricalbin**
159 **family to maintain vacuolar morphology**
160 Tcb3p possesses an N-terminal TM domain, a central SMP domain, and multiple C-terminal C2
161 domains (Fig 2A). To identify which domain of Tcb3p is essential for regulating vacuole fission, we
162 replaced the C-terminal cytoplasmatic sequence of Tcb3p with a GFP binding protein (GBP). This

163 way, we created three strains expressing either full-length Tcb3-GBP; Tcb3(Full)-GBP, Tcb3-GBP
164 lacking C2 domains; Tcb3(TM-SMP)-GBP or Tcb3-GBP lacking both SMP and C2 domains;
165 Tcb3(TM)-GBP. Vacuole morphology in cells expressing Tcb3(Full)-GBP (Fig 2B (iii)) was almost
166 similar to that in WT cells (Fig 2B (i)), indicating that the addition of GBP has no effect on vacuole
167 morphology. Remarkably, vacuoles remained non-fragmented even in cells expressing Tcb3(TM)-
168 GBP, which lacked most of the C-terminal region (Fig 2B (v)), as well as Tcb3(TM-SMP)-GBP (Fig
169 2B (iv)). In an attempt to address the question of why the TM domain of Tcb3p is sufficient to
170 suppress vacuolar division, we found that cells expressing Tcb3(TM)-GBP and lacking Tcb1p and
171 Tcb2p (Fig 2B (vi)) showed vacuolar fragmentation to the same extent as *tcb3*Δ mutant cells (Fig
172 2B (ii)). These results suggest that the TM domain of Tcb3p requires Tcb1p and Tcb2p to suppress
173 vacuole fission. According to the structural simulation by AlphaFold2, each TM domain of Tcb1p,
174 Tcb2p, and Tcb3p formed alpha-helical structure, which is known to be typical for membrane
175 proteins (Fig 2C). It is likely that Tcb1p and Tcb2p directly interact with Tcb3p by their TM domains.
176 Interestingly, the complex of these three TM domains was constructed with Tcb3p between Tcb1p
177 and Tcb2p in most cases (Fig 2D). Together these data suggest that the TM domain of Tcb3p
178 contributes sufficiently to the maintenance of vacuolar morphology by mediating the tricalbin
179 complex formation (Fig 2E).
180
181 **Accumulated phytosphingosine in tricalbin-deleted cells causes vacuole fragmentation.**
182 To understand how the deletion of tricalbins leads to vacuole fragmentation, we examined
183 the involvement of lipids. Previous reports showed that levels of ceramides and acylceramides
184 increased in *tcb1*Δ*2*Δ*3*Δ cells [37], and levels of long-chain bases (LCBs) increased in Δtether cells
185 lacking six ER-PM tethering proteins [47]. Here we measured lipids in *tcb1*Δ*2*Δ*3*Δ cells by in vivo
186 labeling with [^{3}H] dihydrosphingosine (DHS), which is a precursor of phytosphingosine (PHS), and
187 observed significant increases in ceramide, phosphatidylethanolamine (PE), PHS,
188 phosphatidylinositol (PI), complex sphingolipids such as inositolphosphorylceramide (IPC) and
189 mannosyl-inositolphosphorylceramide (MIPC) and LCB-1P (DHS-1P/PHS-1P) levels (Fig 3A).
190 We first tested whether increased levels of PHS cause vacuolar fragmentation. Loss of
191 ceramide synthases could cause an increase in PHS levels. Our analysis showed that vacuoles
192 are fragmented in *lag1*Δ*lac1*Δ cells, which lack both enzymes for LCBs (DHS and PHS) conversion
193 into ceramides (Fig 3B). This suggests that ceramide precursors, LCBs or LCB-1P, can induce
194 vacuolar fragmentation. Therefore, we tested if exogenously added PHS induces vacuolar
195 fragmentation in WT cells. As shown in Fig 3C, exogenous addition of PHS induced vacuolar
196 fragmentation. PHS are converted into ceramide by the ceramide synthase Lag1p, which is the
197 main enzyme synthesizing phytoceramide [48]. Thus, we next examined whether PHS-induced
198 vacuolar fragmentation occurs in *lag1*Δ cells. Our analysis showed that vacuolar fragmentation in

199 *lag1*Δ cells treated with PHS was comparable to that for WT cells (Fig 3C). These results confirm
200 that the increases in ceramide and subsequent product IPC/MIPC are not the cause of vacuolar
201 fragmentation, but rather its precursors induce vacuolar fragmentation.
202 Because our lipid analysis showed a strong increase in LCB-1P in *tcb1*Δ*2*Δ*3*Δ cells,
203 phosphorylation of PHS may be involved in PHS-induced vacuolar fragmentation. Although
204 exogenously added LCBs move slowly from the PM to the ER if they are not phosphorylated,
205 efficient utilization of exogenously added LCBs in sphingolipid synthesis requires a series of
206 phosphorylation and dephosphorylation steps for LCBs [49]. The major yeast LCB phosphate
207 phosphatase Lcb3p dephosphorylates LCB-1P (DHS-1P/PHS-1P) to yield DHS/PHS [50], while
208 Lcb4p and Lcb5p catalyze the reverse reaction producing DHS-1P/PHS-1P [51]. Lcb3p, Lcb4p,
209 and Lcb5p are localized to the ER, PM or Golgi [49] [52] [53] [54]. We examined the ability of
210 exogenous PHS to fragment vacuoles in cells lacking these processing factors. Our results showed
211 that PHS-induced vacuolar fragmentation was completely blocked in the *lcb3*Δ cells in which PHS-
212 1P is not dephosphorylated (Fig 3D), suggesting that PHS-induced vacuolar fragmentation requires
213 the reaction of dephosphorylation of PHS-1P by Lcb3p. On the other hand, we observed that
214 vacuoles were still fragmented in *lcb4*Δ *lcb5*Δ and *lcb3*Δ *lcb4*Δ *lcb5*Δ cells (Fig 3D). These results
215 suggest that elevated levels of non-phosphorylated PHS induces vacuolar fragmentation (Fig 3E).
216 Additionally, we tested whether overexpression of Rsb1p, which has been reported as a
217 translocase that exports LCBs from the inner to the outer leaflet of the PM [55], rescues vacuole
218 fragmentation in *tcb1*Δ*2*Δ*3*Δ cells. As shown in Fig 3F, we observed that Rsb1p overexpression
219 results in decreased vacuole fragmentation. Collectively, these results support the model in which
220 vacuole fragmentation in tricalbin-deleted cells is caused by increased levels of PHS.
221
222
223 **The nucleus-vacuole junction is required for PHS- or *tcb3*Δ-induced vacuole fragmentation**
224 To characterize further the relationship between PHS and vacuole morphology, we asked
225 whether PHS delivered from the ER to the vacuole induces vacuole fragmentation. We
226 hypothesized that if PHS are transported to the vacuole by either the vesicular transport pathway
227 through the Golgi apparatus or the non-vesicular transport pathway via inter-organellar MCS
228 triggers vacuole fission, then blockage of the transport could rescue the PHS-induced vacuole
229 fragmentation. Accordingly, we used two types of mutant strains, one blocking vesicular transport
230 and the other blocking the NVJ. In a temperature sensitive *sec18-20* mutant, vesicular transport is
231 abolished at the restrictive temperature of 30 ºC or higher, but even at the permissive temperature
232 of 25 ºC, vesicular transport is partially impaired [56]. As shown in Fig 4A (left), under the condition
233 without exogenous PHS, some vacuoles in *sec18-20* mutant cells became fragmented when shifted
234 to the non-permissive temperature of 30 ºC. We also observed that vacuoles in *sec18-20* mutant

235 at 30 ºC underwent fragmentation after addition of PHS to the same extent as at the permissive
236 temperature of 25 ºC (Fig 4A, right), suggesting that vesicle-mediated transport is not required for
237 PHS-induced vacuolar fragmentation. To test the role of NVJ-mediated transport for PHS-induced
238 vacuolar fragmentation we employed a quadruple Δ*NVJ* mutant (*nvj1*Δ *nvj2*Δ *nvj3*Δ *mdm1*Δ) that
239 was used in a previous study in which complete loss of the NVJ was observed [57], but thus has
240 a different background to other strains of this study. When PHS was added to the Δ*NVJ* mutant,
241 we observed a significant suppression of vacuole fragmentation compared to WT (Fig 4B). Finally,
242 to investigate the requirement for NVJ in tricalbin deletion-induced vacuolar fragmentation, we
243 constructed the *tcb3*Δ *nvj1*Δ and *tcb*3Δ *nvj1*Δ *nvj2*Δ *nvj3*Δ *mdm1*Δ mutants. *TCB3* single disruption
244 sufficiently induced vacuolar fragmentation (Fig 1B), whereas as expected, the fragmentation was
245 partially suppressed by loss of only *NVJ1* and completely suppressed by loss of all NVJ factors
246 (*NVJ1*, *NVJ2*, *NVJ3*, and *MDM1*) (Fig 4C). Taken together, we conclude from these findings that
247 accumulated PHS in tricalbin deleted cells triggers vacuole fission via non-vesicular transport of
248 PHS at the NVJ.
249
250
251 **Discussion**
252
253 In the present study, we found that the accumulation of PHS triggers the fission of vacuoles.
254 Our results suggest that MCSs are involved in this process in two steps. First, the intracellular
255 amount of PHS is modulated by tricalbin-tethered MCSs between the ER and PM or Golgi (Fig 4D
256 blue arrow). Second, the accumulated PHS in the tricalbin-deleted cells induces vacuole fission
257 via most likely the NVJ (Fig 4D red arrow). Thus, we propose that MCSs regulate vacuole
258 morphology via sphingolipid metabolism. Fundamental questions that arise from our data concern
259 the accumulation of PHS in the tricalbin deletion strain and the mechanism of PHS-induced vacuole
260 fission. Possible mechanisms for elevated PHS levels in tricalbin-deleted cells are the following.
261 MCS deficiency between ER and PM has been shown to reduce the activity of Sac1p, a PtdIns4P
262 phosphatase [36]. Sac1p disruption strain decreases the levels of complex sphingolipids such as
263 IPC and MIPC, while it increases the levels of their precursors, ceramide, LCB, and LCB-1P [58].
264 This is probably due to the loss of function of Sac1p, which reduces the level of PtdIns used for
265 IPC synthesis, thereby impairing IPC synthesis, and resulting in the accumulation of precursors
266 such as the substrate ceramide. This model is also consistent with the results of accumulated
267 PtdIns4P and reduced IPC synthesis in Δtether cells [47]. As tricalbins are required for ceramide
268 nonvesicular transport from the ER to the Golgi [37], it is also possible that impaired ceramide
269 nonvesicular transport due to tricalbin deficiency causes ceramide and its precursor, LCB, to
270 accumulate in the ER. Another possibility is that MCS facilitate PHS diffusion between the ER and

271 the PM, which might be coordinated with the LCB export from the PM by Rsb1p. The loss of
272 tricalbins partially disrupts the ER-PM tether, possibly resulting low efficiency of PHS ejection by
273 Rsb1p. This is supported by the result that overexpression of Rsb1p suppressed vacuolar
274 fragmentation in tricalbin-deleted cells (Fig 3F).

275 Because both PHS- and tricalbin deletion-induced vacuolar fragmentations were partially
276 suppressed by the lack of NVJ (Fig 4B, 4C), it is suggested that transport of PHS into vacuoles via
277 the NVJ is involved in triggering vacuolar fragmentation. Recently, it has been reported that
278 sphingoid bases are transferred between ER and vacuole via the NVJ, and that Mdm1p, a key
279 tethering protein for the formation of the NVJ, may play an additional role in LCB transfer [35].
280 Perhaps, Mdm1p may be responsible for pulling out and passing LCBs. However, we cannot rule
281 out the possibility that the repression of vacuolar fragmentation in the absence of NVJ is not due to
282 inhibition of PHS transfer, but rather to changes in the lipid composition of the vacuolar membrane
283 caused by the lack of supply of other substances capable of triggering vacuolar fragmentation other
284 than PHS, like sterols and lipids such as PtdIns[3,5]P2 and its precursors. Further analysis in this
285 regard is warranted.

286 How accumulated PHS triggers vacuolar fragmentation remains undetermined.
287 Sphingosine, as a bioactive lipid, has been reported to exert effects on enzyme activity in humans
288 and yeast [59] [60] [61], and it is possible that PHS may induce vacuolar fragmentation through
289 established signaling pathways. Yabuki et al [61] reported that LCB accumulation activates a
290 signaling pathway that includes major yeast regulatory kinases such as Pkh1/2p, Pkc1p and
291 TORC1, which may be a candidate to promote vacuolar fragmentation. Fab1p, a target of TORC1,
292 is responsible for the production of PtdIns[3,5]P2, which is a well-established inducer of vacuolar
293 fragmentation. Fab1p exhibits co-localization with the TORC1-activating EGO complex, and its
294 activity is controlled by Ivy1p [62] and TORC1 [63]. PtdIns[3,5]P2 was shown to regulate vacuole
295 fission employing Vps1p and Atg18p as executioners [64] while also promoting TORC1 activity in
296 a positive feedback loop [65]. In this context, we found that PHS-induced vacuolar fragmentation
297 can be suppressed by the loss of Fab1p and its regulatory binding partner Vac14p (Fig S2A). This
298 observation suggests that PHS-induced vacuolar fragmentation requires PI metabolism. On the
299 other hand, it was shown that membrane division is mediated by certain proteins that contain
300 amphipathic helices (AHs) and interact with lipid cofactors such as PtdIns[4,5]P2, PA, and
301 cardiolipin [66]. Thus, PHS may possess a similar regulatory function as a lipid cofactor for the
302 activity of fission-inducing proteins.

303 If PHS-induced vacuole fragmentation is not due to signaling, another possible model is
304 that PHS accumulation in the vacuolar membrane causes physical changes in the membrane
305 structure that result in membrane fragmentation. The accumulation of sphingosine in the of GARP
306 mutant *vps53*Δ, in which retrograde transport from the endosome to the Golgi is blocked, caused

307 vacuolar fragmentation [67], and thus also supports this model. Sphingosine stabilizes (rigidifies)
308 the gel domains in the membrane, leading to a structural defect between the phase separation of
309 "more rigid" and "less rigid" domains [68]. This structural defect may result in high membrane
310 permeability. Sphingosine also forms small and unstable channels (compared to the channels
311 formed by ceramide) in the membrane [69]. Sphingosine channels are not large enough to release
312 proteins, but are believed to induce a permeability transition. Other studies have suggested that
313 sphingosine induces non-lamellar structures by interacting with negatively charged lipids such as
314 PA [70]. Finally, PHS alone or in concert with negatively charged lipids such as PtdIns[3,5]P2 may
315 be actively involved in the fission process by inducing structural changes in the vacuolar
316 membrane.
317 Besides PHS-induced vacuolar fission, it is generally well-known that vacuolar division can
318 be triggered as an acute response to osmotic shock. We made an interesting observation under
319 hyperosmotic conditions (0.2 M NaCl), wherein the loss of NVJ led to complete suppression of
320 vacuolar division (Fig S2B). Although the involvement of PHS transport in this process remains
321 unclear, our finding suggests a significant role for NVJ in vacuolar fission as a hyperosmotic
322 response. Collectively, we propose that NVJ plays a general regulatory role in vacuolar
323 morphology.
324
325
326
327 **Materials and Methods**
328
329 **Yeast strains**
330 All strains of *S. cerevisiae* used for this work are listed in Supplementary Table 1.
331
332 **Plasmids**
333 All plasmids used for this work are listed in Supplementary Table 2.
334
335 **Culture conditions**
336 Yeast cells were grown either in rich YPD medium (2% glucose, 1% yeast extract, 2% peptone) or
337 in synthetic minimal SD medium (2% glucose, 0.15% yeast nitrogen base, 0.5% ammonium sulfate,
338 bases as nutritional requirements) and supplemented with the appropriate amino acids.
339
340 **FM4-64 stain and Fluorescence Microscopy**
341 Yeast cells were cultured in YPD medium at 25°C for 15 hours to achieve OD_{600} = 0.5. The cells
342 were collected and suspended in the same medium to achieve OD_{600}=20. 20 mM FM4-64 (N-(3-

343 Triethylammoniumpropyl)-4-(6-(4-(diethylamino) phenyl) hexatrienyl) pyridinium) dissolved in
344 DMSO was added (a final concentration of 20 μM) while shielded from light. The cells were
345 incubated with FM4-64 for 15 minutes at 25°C and then the cells were washed twice with YPD
346 medium. Cells were suspended to achieve OD_{600}=10 in the same YPD medium or YPD containing
347 reagents (such as rapamycin or PHS), and incubated at 25°C for 2 hours under light shielding to
348 label the vacuoles. After incubation, cells were collected and observed with a fluorescence
349 microscope.
350
351 **Western Blotting**
352 To analyze Sch9 phosphorylation, protein extracts from cells expressing SCH9-5HA were treated
353 with 2-nitro-5-thiocyanobenzoic acid overnight, resolved by SDS-PAGE, immunoblotted, and
354 visualized using rat anti-HA monoclonal antibody (3F10; Roche) and anti-rat IgG antibody (A9037;
355 Sigma-Aldrich) produced in goat. Bands were quantified using ImageJ to determine the relative
356 amounts of phosphorylated Sch9.
357
358 **Lipid Labelling with [^{3}H]DHS**
359 In vivo labelling of lipids with [^{3}H]DHS was carried out as described [71]. Radiolabeled lipids were
360 extracted with chloroform-methanol-water (10:10:3, vol/vol/vol), and analyzed by thin-layer
361 chromatography (TLC) using a solvent system (Chloroform-methanol-4.2N ammonium hydroxide
362 (9:7:2, vol/vol/vol)). Radiolabeled lipids were visualized and quantified on an FLA-7000 system.
363
364 **Protein complex modelling**
365 The modeled Tcb1p, Tcb2p, and Tcb3p structures were obtained from AlphaFold2 Protein
366 Structure Database (https://alphafold.ebi.ac.uk/). Based on the modeled structures, the amino
367 acids of TM regions were predicted as 79-171 for Tcb1p, 79-162 for Tcb2p, and 189-268 for Tcb3p.
368 The protein complex structures of the TM regions in Tcb1p, Tcb2p, and Tcb3p were modelled by
369 AlphaFold2 program [72] worked on the AlphaFold Colab web space
370 (https://colab.research.google.com/github/deepmind/alphafold/blob/main/notebooks/AlphaFold.ipy
371 nb#scrollTo=pc5-mbsX9PZC). The figures were drawn using PyMOL software provided by
372 Schrödinger, Inc. (https://pymol.org/2/).
373
374
375 **Data and Materials Availability Statement**
376 The data and materials that support the findings of this study are included in the article and its
377 Supplemental Information, or are available from the corresponding authors on request.
378

Acknowledgments

We thank Takashi Toda and Masashi Yukawa for GBP-plasmid, Mike Henne for the Δ*NVJ* strain, and Howard Riezman for GFP-CPS1 plasmid. This research was supported by JSPS KAKENHI 21K20572 and 22K14863 to A.I., 19H02922 and 21K19088 to K.F.

Author Contributions

K.N., A.I. and K.F. designed research; K.H., K. N., A.I., S.Y., A.N. and S.F. performed research; A.I. analyzed data; and A.I., P.S. and K.F. wrote the paper.

Competing Interest Statement

The authors declare no competing interest.

References

1. Baars, T. L., Petri, S., Peters, C., & Mayer, A. (2007). Role of the V-ATPase in regulation of the vacuolar fission-fusion equilibrium. *Molecular biology of the cell*, *18*(10), 3873–3882. doi:10.1091/mbc.e07-03-0205. https://doi.org/10.1091/mbc.e07-03-0205
2. Li, S. C., & Kane, P. M. (2009). The yeast lysosome-like vacuole: endpoint and crossroads. *Biochimica et biophysica acta*, *1793*(4), 650–663. doi:10.1016/j.bbamcr.2008.08.003. https://doi.org/10.1016/j.bbamcr.2008.08.003
3. Wickner, W., & Haas, A. (2000). Yeast homotypic vacuole fusion: a window on organelle trafficking mechanisms. *Annual review of biochemistry*, *69*, 247–275. doi:10.1146/annurev.biochem.69.1.247. https://doi.org/10.1146/annurev.biochem.69.1.247
4. Ostrowicz, C. W., Meiringer, C. T., & Ungermann, C. (2008). Yeast vacuole fusion: a model system for eukaryotic endomembrane dynamics. *Autophagy*, *4*(1), 5–19. doi:10.4161/auto.5054. https://doi.org/10.4161/auto.5054
5. Wickner W. (2010). Membrane fusion: five lipids, four SNAREs, three chaperones, two nucleotides, and a Rab, all dancing in a ring on yeast vacuoles. *Annual review of cell and*

411 *developmental biology*, *26*, 115–136. doi:10.1146/annurev-cellbio-100109-104131.
412 https://doi.org/10.1146/annurev-cellbio-100109-104131
413 6. Qiu Q. S. (2012). V-ATPase, ScNhx1p and yeast vacuole fusion. *Journal of genetics and*
414 *genomics = Yi chuan xue bao*, *39*(4), 167–171. doi:10.1016/j.jgg.2012.02.001.
415 https://doi.org/10.1016/j.jgg.2012.02.001
416 7. Müller, O., Bayer, M. J., Peters, C., Andersen, J. S., Mann, M., & Mayer, A. (2002). The Vtc
417 proteins in vacuole fusion: coupling NSF activity to V(0) trans-complex formation. *The*
418 *EMBO journal*, *21*(3), 259–269. doi:10.1093/emboj/21.3.259.
419 https://doi.org/10.1093/emboj/21.3.259
420 8. Ho, R., & Stroupe, C. (2016). The HOPS/Class C Vps Complex Tethers High-Curvature
421 Membranes via a Direct Protein-Membrane Interaction. *Traffic (Copenhagen,*
422 *Denmark)*, *17*(10), 1078–1090. doi:10.1111/tra.12421.
423 https://doi.org/10.1111/tra.12421
424 9. Ungermann, C., Wickner, W., & Xu, Z. (1999). Vacuole acidification is required for trans-
425 SNARE pairing, LMA1 release, and homotypic fusion. *Proceedings of the National*
426 *Academy of Sciences of the United States of America*, *96*(20), 11194–11199.
427 doi:10.1073/pnas.96.20.11194. https://doi.org/10.1073/pnas.96.20.11194
428 10. Peters, C., Bayer, M. J., Bühler, S., Andersen, J. S., Mann, M., & Mayer, A. (2001). Trans-
429 complex formation by proteolipid channels in the terminal phase of membrane
430 fusion. *Nature*, *409*(6820), 581–588. doi:10.1038/35054500.
431 https://doi.org/10.1038/35054500
432 11. Desfougères, Y., Vavassori, S., Rompf, M., Gerasimaite, R., & Mayer, A. (2016). Organelle
433 acidification negatively regulates vacuole membrane fusion in vivo. *Scientific reports*, *6*,
434 29045. doi:10.1038/srep29045. https://doi.org/10.1038/srep29045
435 12. Starai, V. J., Thorngren, N., Fratti, R. A., & Wickner, W. (2005). Ion regulation of homotypic
436 vacuole fusion in Saccharomyces cerevisiae. *The Journal of biological chemistry*, *280*(17),
437 16754–16762. doi:10.1074/jbc.M500421200. https://doi.org/10.1074/jbc.M500421200
438 13. Qiu, Q. S., & Fratti, R. A. (2010). The Na+/H+ exchanger Nhx1p regulates the initiation of
439 Saccharomyces cerevisiae vacuole fusion. *Journal of cell science*, *123*(Pt 19), 3266–3275.
440 doi:10.1242/jcs.067637. https://doi.org/10.1242/jcs.067637

441 14. Zieger, M., & Mayer, A. (2012). Yeast vacuoles fragment in an asymmetrical two-phase
442 process with distinct protein requirements. *Molecular biology of the cell*, *23*(17), 3438–
443 3449. doi:10.1091/mbc.E12-05-0347. https://doi.org/10.1091/mbc.E12-05-0347
444 15. Peters, C., Baars, T. L., Bühler, S., & Mayer, A. (2004). Mutual control of membrane fission
445 and fusion proteins. *Cell*, *119*(5), 667–678. doi:10.1016/j.cell.2004.11.023.
446 https://doi.org/10.1016/j.cell.2004.11.023
447 16. Weisman L. S. (2006). Organelles on the move: insights from yeast vacuole
448 inheritance. *Nature reviews. Molecular cell biology*, *7*(4), 243–252. doi:10.1038/nrm1892.
449 https://doi.org/10.1038/nrm1892
450 17. Efe, J. A., Botelho, R. J., & Emr, S. D. (2005). The Fab1 phosphatidylinositol kinase pathway
451 in the regulation of vacuole morphology. *Current opinion in cell biology*, *17*(4), 402–408.
452 doi:10.1016/j.ceb.2005.06.002. https://doi.org/10.1016/j.ceb.2005.06.002
453 18. Efe, J. A., Botelho, R. J., & Emr, S. D. (2007). Atg18 regulates organelle morphology and
454 Fab1 kinase activity independent of its membrane recruitment by phosphatidylinositol
455 3,5-bisphosphate. *Molecular biology of the cell*, *18*(11), 4232–4244.
456 doi:10.1091/mbc.e07-04-0301. https://doi.org/10.1091/mbc.e07-04-0301
457 19. Michaillat, L., Baars, T. L., & Mayer, A. (2012). Cell-free reconstitution of vacuole
458 membrane fragmentation reveals regulation of vacuole size and number by
459 TORC1. *Molecular biology of the cell*, *23*(5), 881–895. doi:10.1091/mbc.E11-08-0703.
460 https://doi.org/10.1091/mbc.E11-08-0703
461 20. Stauffer, B., & Powers, T. (2015). Target of rapamycin signaling mediates vacuolar fission
462 caused by endoplasmic reticulum stress in Saccharomyces cerevisiae. *Molecular biology*
463 *of the cell*, *26*(25), 4618–4630. doi:10.1091/mbc.E15-06-0344.
464 https://doi.org/10.1091/mbc.E15-06-0344
465 21. Manandhar, S. P., Siddiqah, I. M., Cocca, S. M., & Gharakhanian, E. (2020). A kinase
466 cascade on the yeast lysosomal vacuole regulates its membrane dynamics: conserved
467 kinase Env7 is phosphorylated by casein kinase Yck3. *The Journal of biological*
468 *chemistry*, *295*(34), 12262–12278. doi:10.1074/jbc.RA119.012346.
469 https://doi.org/10.1074/jbc.RA119.012346

470 22. Wu, H., Carvalho, P., & Voeltz, G. K. (2018). Here, there, and everywhere: The importance
471 of ER membrane contact sites. *Science (New York, N.Y.)*, *361*(6401), eaan5835.
472 doi:10.1126/science.aan5835. https://doi.org/10.1126/science.aan5835
473 23. Prinz, W. A., Toulmay, A., & Balla, T. (2020). The functional universe of membrane contact
474 sites. *Nature reviews. Molecular cell biology*, *21*(1), 7–24. doi:10.1038/s41580-019-0180-
475 9. https://doi.org/10.1038/s41580-019-0180-9
476 24. Wickner, W., & Rizo, J. (2017). A cascade of multiple proteins and lipids catalyzes
477 membrane fusion. *Molecular biology of the cell*, *28*(6), 707–711. doi:10.1091/mbc.E16-
478 07-0517. https://doi.org/10.1091/mbc.E16-07-0517
479 25. Starr, M. L., & Fratti, R. A. (2019). The Participation of Regulatory Lipids in Vacuole
480 Homotypic Fusion. *Trends in biochemical sciences*, *44*(6), 546–554.
481 doi:10.1016/j.tibs.2018.12.003. https://doi.org/10.1016/j.tibs.2018.12.003
482 26. Ungermann, C., & Kümmel, D. (2019). Structure of membrane tethers and their role in
483 fusion. *Traffic (Copenhagen, Denmark)*, *20*(7), 479–490. doi:10.1111/tra.12655.
484 https://doi.org/10.1111/tra.12655
485 27. Hurst, L. R., & Fratti, R. A. (2020). Lipid Rafts, Sphingolipids, and Ergosterol in Yeast
486 Vacuole Fusion and Maturation. *Frontiers in cell and developmental biology*, *8*, 539.
487 doi:10.3389/fcell.2020.00539. https://doi.org/10.3389/fcell.2020.00539
488 28. Pan, X., Roberts, P., Chen, Y., Kvam, E., Shulga, N., Huang, K., Lemmon, S., & Goldfarb, D.
489 S. (2000). Nucleus-vacuole junctions in Saccharomyces cerevisiae are formed through the
490 direct interaction of Vac8p with Nvj1p. *Molecular biology of the cell*, *11*(7), 2445–2457.
491 doi:10.1091/mbc.11.7.2445. https://doi.org/10.1091/mbc.11.7.2445
492 29. Elbaz-Alon, Y., Rosenfeld-Gur, E., Shinder, V., Futerman, A. H., Geiger, T., & Schuldiner, M.
493 (2014). A dynamic interface between vacuoles and mitochondria in yeast. *Developmental*
494 *cell*, *30*(1), 95–102. doi:10.1016/j.devcel.2014.06.007.
495 https://doi.org/10.1016/j.devcel.2014.06.007
496 30. Hönscher, C., Mari, M., Auffarth, K., Bohnert, M., Griffith, J., Geerts, W., van der Laan, M.,
497 Cabrera, M., Reggiori, F., & Ungermann, C. (2014). Cellular metabolism regulates contact
498 sites between vacuoles and mitochondria. *Developmental cell*, *30*(1), 86–94.
499 doi:10.1016/j.devcel.2014.06.006. https://doi.org/10.1016/j.devcel.2014.06.006

31. González Montoro, A., Auffarth, K., Hönscher, C., Bohnert, M., Becker, T., Warscheid, B., Reggiori, F., van der Laan, M., Fröhlich, F., & Ungermann, C. (2018). Vps39 Interacts with Tom40 to Establish One of Two Functionally Distinct Vacuole-Mitochondria Contact Sites. *Developmental cell*, *45*(5), 621–636.e7. doi:10.1016/j.devcel.2018.05.011. https://doi.org/10.1016/j.devcel.2018.05.011
32. Murley, A., Sarsam, R. D., Toulmay, A., Yamada, J., Prinz, W. A., & Nunnari, J. (2015). Ltc1 is an ER-localized sterol transporter and a component of ER-mitochondria and ER-vacuole contacts. *The Journal of cell biology*, *209*(4), 539–548. doi:10.1083/jcb.201502033. https://doi.org/10.1083/jcb.201502033
33. Murley, A., Yamada, J., Niles, B. J., Toulmay, A., Prinz, W. A., Powers, T., & Nunnari, J. (2017). Sterol transporters at membrane contact sites regulate TORC1 and TORC2 signaling. *The Journal of cell biology*, *216*(9), 2679–2689.
34. Reinisch, K. M., & Prinz, W. A. (2021). Mechanisms of nonvesicular lipid transport. *The Journal of cell biology*, *220*(3), e202012058. doi:10.1083/jcb.201610032. https://doi.org/10.1083/jcb.201610032
35. Girik, V., Feng, S., Hariri, H., Henne, W. M., & Riezman, H. (2022). Vacuole-Specific Lipid Release for Tracking Intracellular Lipid Metabolism and Transport in Saccharomyces cerevisiae. *ACS chemical biology*, 17(6), 1485–1494. doi:10.1021/acschembio.2c00120. https://doi.org/10.1021/acschembio.2c00120
36. Manford, A. G., Stefan, C. J., Yuan, H. L., Macgurn, J. A., & Emr, S. D. (2012). ER-to-plasma membrane tethering proteins regulate cell signaling and ER morphology. *Developmental cell*, *23*(6), 1129–1140. doi:10.1016/j.devcel.2012.11.004. https://doi.org/10.1016/j.devcel.2012.11.004
37. Ikeda, A., Schlarmann, P., Kurokawa, K., Nakano, A., Riezman, H., & Funato, K. (2020). Tricalbins Are Required for Non-vesicular Ceramide Transport at ER-Golgi Contacts and Modulate Lipid Droplet Biogenesis. *iScience*, *23*(10), 101603. doi:10.1016/j.isci.2020.101603. https://doi.org/10.1016/j.isci.2020.101603
38. Toulmay, A., & Prinz, W. A. (2012). A conserved membrane-binding domain targets proteins to organelle contact sites. *Journal of cell science*, *125*(Pt 1), 49–58. doi:10.1242/jcs.085118. https://doi.org/10.1242/jcs.085118

530 39. Quon, E., Sere, Y. Y., Chauhan, N., Johansen, J., Sullivan, D. P., Dittman, J. S., Rice, W. J.,
531 Chan, R. B., Di Paolo, G., Beh, C. T., & Menon, A. K. (2018). Endoplasmic reticulum-plasma
532 membrane contact sites integrate sterol and phospholipid regulation. *PLoS biology*, *16*(5),
533 e2003864. doi:10.1371/journal.pbio.2003864.
534 https://doi.org/10.1371/journal.pbio.2003864
535 40. Jorgensen, J. R., Tei, R., Baskin, J. M., Michel, A. H., Kornmann, B., & Emr, S. D. (2020).
536 ESCRT-III and ER-PM contacts maintain lipid homeostasis. *Molecular biology of the cell*,
537 *31*(12), 1302–1313. doi:10.1091/mbc.E20-01-0061. https://doi.org/10.1091/mbc.E20-
538 01-0061
539 41. Hoffmann, P. C., Bharat, T., Wozny, M. R., Boulanger, J., Miller, E. A., & Kukulski, W. (2019).
540 Tricalbins Contribute to Cellular Lipid Flux and Form Curved ER-PM Contacts that Are
541 Bridged by Rod-Shaped Structures. *Developmental cell*, *51*(4), 488–502.e8.
542 doi:10.1016/j.devcel.2019.09.019. https://doi.org/10.1016/j.devcel.2019.09.019
543 42. Collado, J., Kalemanov, M., Campelo, F., Bourgoint, C., Thomas, F., Loewith, R., Martínez-
544 Sánchez, A., Baumeister, W., Stefan, C. J., & Fernández-Busnadiego, R. (2019). Tricalbin-
545 Mediated Contact Sites Control ER Curvature to Maintain Plasma Membrane Integrity.
546 *Developmental cell*, 51(4), 476–487.e7. doi:10.1016/j.devcel.2019.10.018.
547 https://doi.org/10.1016/j.devcel.2019.10.018
548 43. Nelson, H., & Nelson, N. (1990). Disruption of genes encoding subunits of yeast vacuolar
549 H(+)-ATPase causes conditional lethality. *Proceedings of the National Academy of*
550 *Sciences of the United States of America*, *87*(9), 3503–3507. doi:10.1073/pnas.87.9.3503.
551 https://doi.org/10.1073/pnas.87.9.3503
552 44. Coonrod, E. M., Graham, L. A., Carpp, L. N., Carr, T. M., Stirrat, L., Bowers, K., Bryant, N. J.,
553 & Stevens, T. H. (2013). Homotypic vacuole fusion in yeast requires organelle acidification
554 and not the V-ATPase membrane domain. *Developmental cell*, *27*(4), 462–468.
555 doi:10.1016/j.devcel.2013.10.014. https://doi.org/10.1016/j.devcel.2013.10.014
556 45. Seeley, E. S., Kato, M., Margolis, N., Wickner, W., & Eitzen, G. (2002). Genomic analysis of
557 homotypic vacuole fusion. *Molecular biology of the cell*, *13*(3), 782–794.
558 doi:10.1091/mbc.01-10-0512. https://doi.org/10.1091/mbc.01-10-0512
559 46. Dove, S. K., Dong, K., Kobayashi, T., Williams, F. K., & Michell, R. H. (2009).
560 Phosphatidylinositol 3,5-bisphosphate and Fab1p/PIKfyve underPPIn endo-lysosome

561 function. *The Biochemical journal*, *419*(1), 1–13. doi:10.1042/BJ20081950.
562 https://doi.org/10.1042/BJ20081950
563 47. Omnus, D. J., Manford, A. G., Bader, J. M., Emr, S. D., & Stefan, C. J. (2016).
564 Phosphoinositide kinase signaling controls ER-PM cross-talk. *Molecular biology of the*
565 *cell*, *27*(7), 1170–1180. doi:10.1091/mbc.E16-01-0002.
566 https://doi.org/10.1091/mbc.E16-01-0002
567 48. Megyeri, M., Prasad, R., Volpert, G., Sliwa-Gonzalez, A., Haribowo, A. G., Aguilera-Romero,
568 A., Riezman, H., Barral, Y., Futerman, A. H., & Schuldiner, M. (2019). Yeast ceramide
569 synthases, Lag1 and Lac1, have distinct substrate specificity. *Journal of cell*
570 *science*, *132*(12), jcs228411. doi:10.1242/jcs.228411. https://doi.org/10.1242/jcs.228411
571 49. Funato, K., Lombardi, R., Vallee, B., & Riezman, H. (2003). Lcb4p is a key regulator of
572 ceramide synthesis from exogenous long chain sphingoid base in Saccharomyces
573 cerevisiae. *The Journal of biological chemistry*, *278*(9), 7325–7334.
574 doi:10.1074/jbc.M209925200. https://doi.org/10.1074/jbc.M209925200
575 50. Qie, L., Nagiec, M. M., Baltisberger, J. A., Lester, R. L., & Dickson, R. C. (1997). Identification
576 of a Saccharomyces gene, LCB3, necessary for incorporation of exogenous long chain
577 bases into sphingolipids. *The Journal of biological chemistry*, *272*(26), 16110–16117.
578 doi:10.1074/jbc.272.26.16110. https://doi.org/10.1074/jbc.272.26.16110
579 51. Nagiec, M. M., Skrzypek, M., Nagiec, E. E., Lester, R. L., & Dickson, R. C. (1998). The LCB4
580 (YOR171c) and LCB5 (YLR260w) genes of Saccharomyces encode sphingoid long chain
581 base kinases. *The Journal of biological chemistry*, *273*(31), 19437–19442.
582 doi:10.1074/jbc.273.31.19437. https://doi.org/10.1074/jbc.273.31.19437
583 52. Mao, C., Saba, J. D., & Obeid, L. M. (1999). The dihydrosphingosine-1-phosphate
584 phosphatases of Saccharomyces cerevisiae are important regulators of cell proliferation
585 and heat stress responses. *The Biochemical journal*, 342 Pt 3(Pt 3), 667–675. PMID:
586 10477278; PMCID: PMC1220508.
587 53. Hait, N. C., Fujita, K., Lester, R. L., & Dickson, R. C. (2002). Lcb4p sphingoid base kinase
588 localizes to the Golgi and late endosomes. *FEBS letters*, 532(1-2), 97–102.
589 doi:10.1016/s0014-5793(02)03636-0. https://doi.org/10.1016/s0014-5793(02)03636-0
590 54. Iwaki, S., Sano, T., Takagi, T., Osumi, M., Kihara, A., & Igarashi, Y. (2007). Intracellular
591 trafficking pathway of yeast long-chain base kinase Lcb4, from its synthesis to its

592 degradation. *The Journal of biological chemistry*, 282(39), 28485–28492.
593 doi:10.1074/jbc.M701607200. https://doi.org/10.1074/jbc.M701607200
594 55. Kihara, A., & Igarashi, Y. (2002). Identification and characterization of a Saccharomyces
595 cerevisiae gene, RSB1, involved in sphingoid long-chain base release. *The Journal of*
596 *biological chemistry*, *277*(33), 30048–30054. doi:10.1074/jbc.M203385200.
597 https://doi.org/10.1074/jbc.M203385200
598 56. Funato, K., & Riezman, H. (2001). Vesicular and nonvesicular transport of ceramide from
599 ER to the Golgi apparatus in yeast. *The Journal of cell biology*, 155(6), 949–959.
600 doi:10.1083/jcb.200105033. https://doi.org/10.1083/jcb.200105033
601 57. Henne, W. M., Zhu, L., Balogi, Z., Stefan, C., Pleiss, J. A., & Emr, S. D. (2015). Mdm1/Snx13
602 is a novel ER-endolysosomal interorganelle tethering protein. *The Journal of cell biology*,
603 210(4), 541–551. doi:10.1083/jcb.201503088. https://doi.org/10.1083/jcb.201503088
604 58. Brice, S. E., Alford, C. W., & Cowart, L. A. (2009). Modulation of sphingolipid metabolism
605 by the phosphatidylinositol-4-phosphate phosphatase Sac1p through regulation of
606 phosphatidylinositol in Saccharomyces cerevisiae. *The Journal of biological*
607 *chemistry*, *284*(12), 7588–7596. doi:10.1074/jbc.M808325200.
608 https://doi.org/10.1074/jbc.M808325200
609 59. Hannun, Y. A., Loomis, C. R., Merrill, A. H., Jr, & Bell, R. M. (1986). Sphingosine inhibition
610 of protein kinase C activity and of phorbol dibutyrate binding in vitro and in human
611 platelets. *The Journal of biological chemistry*, *261*(27), 12604–12609. PMID: 3462188.
612 60. Chang, H. C., Tsai, L. H., Chuang, L. Y., & Hung, W. C. (2001). Role of AKT kinase in
613 sphingosine-induced apoptosis in human hepatoma cells. *Journal of cellular*
614 *physiology*, *188*(2), 188–193. doi:10.1002/jcp.1108. https://doi.org/10.1002/jcp.1108
615 61. Yabuki, Y., Ikeda, A., Araki, M., Kajiwara, K., Mizuta, K., & Funato, K. (2019).
616 Sphingolipid/Pkh1/2-TORC1/Sch9 Signaling Regulates Ribosome Biogenesis in
617 Tunicamycin-Induced Stress Response in Yeast. *Genetics*, *212*(1), 175–186.
618 doi:10.1534/genetics.118.301874. https://doi.org/10.1534/genetics.118.301874
619 62. Malia, P. C., Numrich, J., Nishimura, T., González Montoro, A., Stefan, C. J., & Ungermann,
620 C. (2018). Control of vacuole membrane homeostasis by a resident PI-3,5-kinase
621 inhibitor. *Proceedings of the National Academy of Sciences of the United States of*

America, *115*(18), 4684–4689. doi:10.1073/pnas.1722517115. https://doi.org/10.1073/pnas.1722517115

63. Chen, Z., Malia, P. C., Hatakeyama, R., Nicastro, R., Hu, Z., Péli-Gulli, M. P., Gao, J., Nishimura, T., Eskes, E., Stefan, C. J., Winderickx, J., Dengjel, J., De Virgilio, C., & Ungermann, C. (2021). TORC1 Determines Fab1 Lipid Kinase Function at Signaling Endosomes and Vacuoles. *Current biology : CB*, *31*(2), 297–309.e8. doi:10.1016/j.cub.2020.10.026. https://doi.org/10.1016/j.cub.2020.10.026
64. Gopaldass, N., Fauvet, B., Lashuel, H., Roux, A., & Mayer, A. (2017). Membrane scission driven by the PROPPIN Atg18. *The EMBO journal*, *36*(22), 3274–3291. doi:10.15252/embj.201796859. https://doi.org/10.15252/embj.201796859
65. Jin, N., Mao, K., Jin, Y., Tevzadze, G., Kauffman, E. J., Park, S., Bridges, D., Loewith, R., Saltiel, A. R., Klionsky, D. J., & Weisman, L. S. (2014). Roles for PI(3,5)P2 in nutrient sensing through TORC1. *Molecular biology of the cell*, *25*(7), 1171–1185. doi:10.1091/mbc.E14-01-0021. https://doi.org/10.1091/mbc.E14-01-0021
66. Zhukovsky, M. A., Filograna, A., Luini, A., Corda, D., & Valente, C. (2019). Protein Amphipathic Helix Insertion: A Mechanism to Induce Membrane Fission. *Frontiers in cell and developmental biology*, *7*, 291. doi:10.3389/fcell.2019.00291. https://doi.org/10.3389/fcell.2019.00291
67. Fröhlich, F., Petit, C., Kory, N., Christiano, R., Hannibal-Bach, H. K., Graham, M., Liu, X., Ejsing, C. S., Farese, R. V., & Walther, T. C. (2015). The GARP complex is required for cellular sphingolipid homeostasis. *eLife*, *4*, e08712. doi:10.7554/eLife.08712. https://doi.org/10.7554/eLife.08712
68. Contreras, F. X., Sot, J., Alonso, A., & Goñi, F. M. (2006). Sphingosine increases the permeability of model and cell membranes. *Biophysical journal*, *90*(11), 4085–4092. doi:10.1529/biophysj.105.076471. https://doi.org/10.1529/biophysj.105.076471
69. Siskind, L. J., Fluss, S., Bui, M., & Colombini, M. (2005). Sphingosine forms channels in membranes that differ greatly from those formed by ceramide. *Journal of bioenergetics and biomembranes*, *37*(4), 227–236. doi:10.1007/s10863-005-6632-2. https://doi.org/10.1007/s10863-005-6632-2
70. Jiménez-Rojo, N., Sot, J., Viguera, A. R., Collado, M. I., Torrecillas, A., Gómez-Fernández, J. C., Goñi, F. M., & Alonso, A. (2014). Membrane permeabilization induced by sphingosine:

effect of negatively charged lipids. *Biophysical journal*, *106*(12), 2577–2584. doi:10.1016/j.bpj.2014.04.038. https://doi.org/10.1016/j.bpj.2014.04.038

71. Ikeda, A., Hanaoka, K., & Funato, K. (2021). Protocol for measuring sphingolipid metabolism in budding yeast. STAR protocols, 2(2), 100412. doi:10.1016/j.xpro.2021.100412. https://doi.org/10.1016/j.xpro.2021.100412

72. Jumper, J., Evans, R., Pritzel, A., Green, T., Figurnov, M., Ronneberger, O., Tunyasuvunakool, K., Bates, R., Žídek, A., Potapenko, A., Bridgland, A., Meyer, C., Kohl, S., Ballard, A. J., Cowie, A., Romera-Paredes, B., Nikolov, S., Jain, R., Adler, J., Back, T., Petersen, S., Reiman, D., Clancy, E., Zielinski, M., Steinegger, M., Pacholska, M., Berghammer, T., Bodenstein, S., Silver, D., Vinyals, O., Senior, A. W., Kavukcuoglu, K., Kohli, P., Hassabis, D., & Hassabis, D. (2021). Highly accurate protein structure prediction with AlphaFold. *Nature*, *596*(7873), 583–589. doi:10.1038/s41586-021-03819-2. https://doi.org/10.1038/s41586-021-03819-2

667 **Figures and legends**

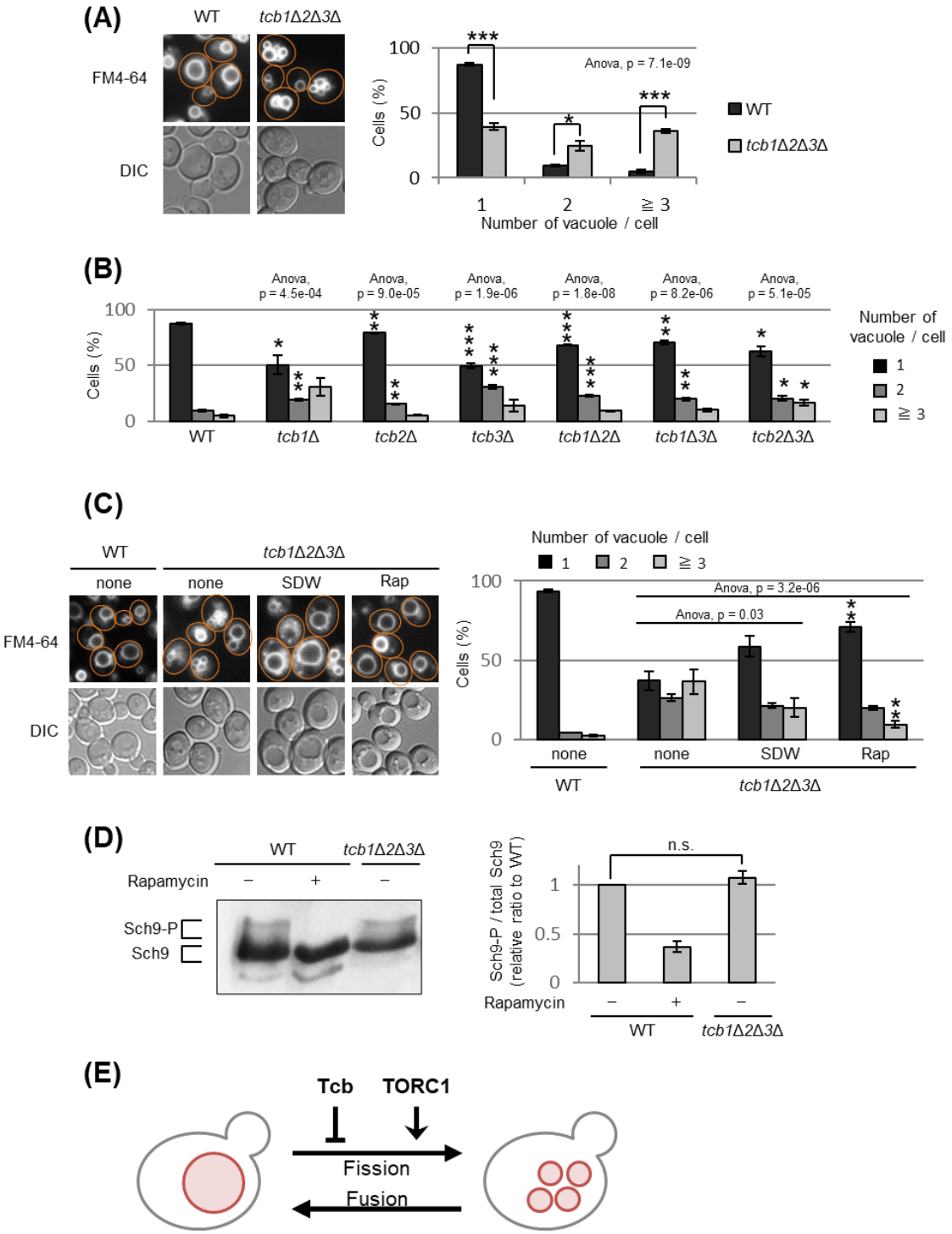

668

669 **Figure 1. Deletion of tricalbin proteins causes vacuole fragmentation**

670 (A, B) Cells (FKY2577 and FKY2927 in A; FKY2577, FKY2909, FKY3819, FKY2924, FKY3023,

671 FKY3820 and FKY3008 in B) were grown overnight at 25 ºC in YPD. Then vacuoles were stained

672 with FM4-64 and imaged by fluorescence microscopy. The number of vacuoles per cell was
673 counted and categorized into one of three groups. The data represent mean ± SE of three
674 independent experiments, each based on more than 100 cells. *p < 0.05, **p < 0.01 and ***p <
675 0.001 by Student's t-test compared with WT.
676 (C) Cells (FKY2577 and FKY2927) were grown overnight at 25 ºC in YPD. Cells were then
677 incubated in sterile distilled water (SDW) for more than 45 minutes or YPD with 200 nM of
678 rapamycin for 2 hours. Vacuoles were stained with FM4-64 and imaged by fluorescence
679 microscopy. The number of vacuoles per cell was counted and categorized into one of three
680 groups. The data represent mean ± SE of seven (SDW) or three (Rap) independent experiments,
681 each based on more than 100 cells. **p < 0.01 by Student's t-test compared with none treated
682 *tcb1*Δ*2*Δ*3*Δ cells.
683 (A-C) Significant differences analysis between the pairwise combination of groups was performed
684 using two-way ANOVA.
685 (D) Cells (FKY2577 and FKY2927) transformed with pRS416-SCH9-5HA were cultured in YPD,
686 treated with 200 nM rapamycin (control) or untreated. The extracts from cells expressing Sch9-
687 5HA were reacted with 2-nitro-5-thiocyanobenzoic acid and analyzed by immunoblotting using anti-
688 HA. Phosphorylated Sch9 relative to the total Sch9 was calculated and shown in comparison to
689 untreated WT cells. The data represent mean ± SE of three independent experiments. *p < 0.05 by
690 Student's t-test.
691 (E) Illustration shows that tricalbin proteins negatively regulate the vacuole fission in a TORC1-
692 independent manner.
693

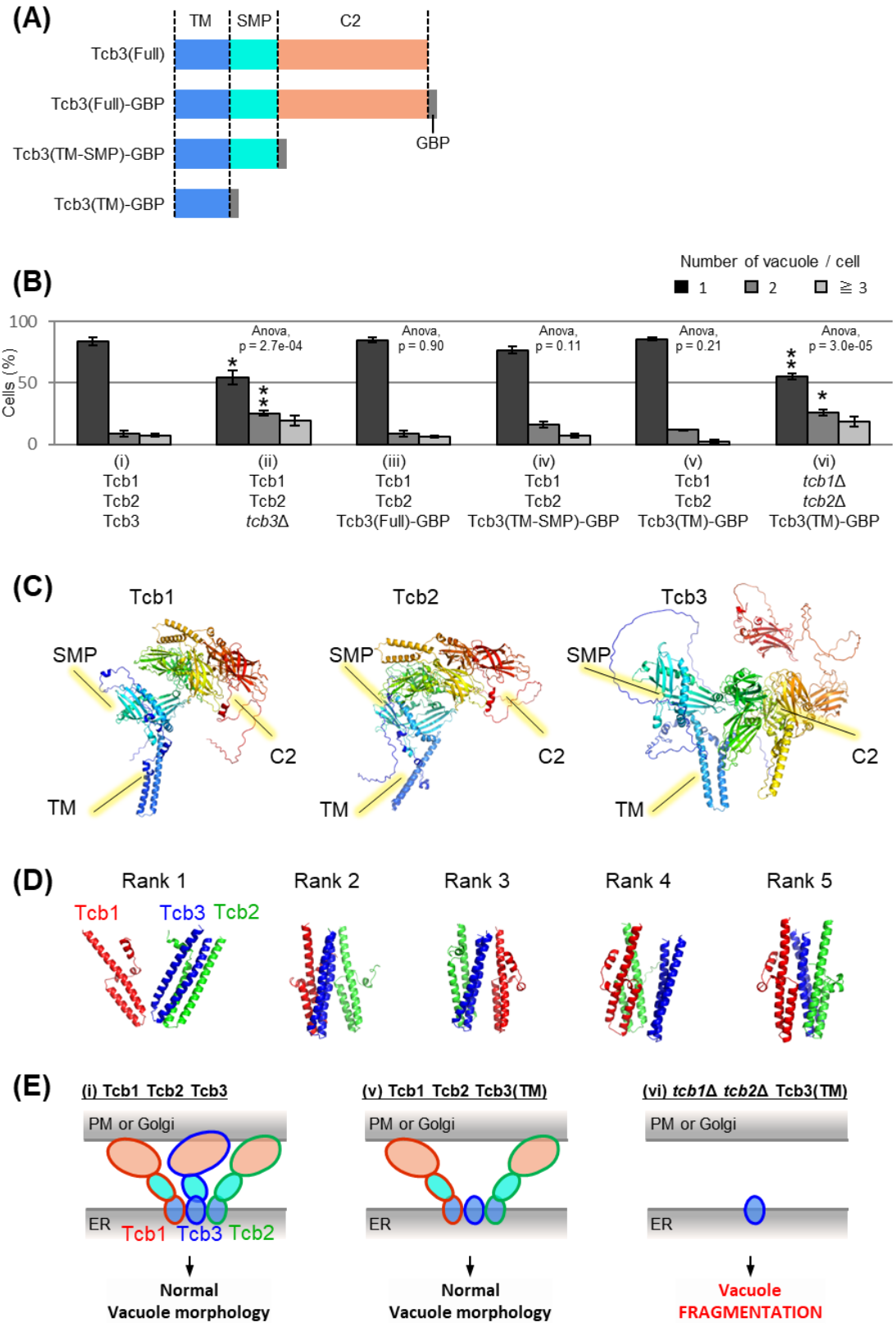
(A)
TM
SMP
C2
Tcb3(Full)
Tcb3(Full)-GBP
GBP
Tcb3(TM-SMP)-GBP
Tcb3(TM)-GBP
(B)
Number of vacuole / cell
1
2
≧ 3
Cells (%)
100
50
0
Anova, p = 2.7e-04
Anova, p = 0.90
Anova, p = 0.11
Anova, p = 0.21
Anova, p = 3.0e-05
(i) Tcb1 Tcb2 Tcb3
(ii) Tcb1 Tcb2 tcb3Δ
(iii) Tcb1 Tcb2 Tcb3(Full)-GBP
(iv) Tcb1 Tcb2 Tcb3(TM-SMP)-GBP
(v) Tcb1 Tcb2 Tcb3(TM)-GBP
(vi) tcb1Δ tcb2Δ Tcb3(TM)-GBP
(C)
Tcb1
Tcb2
Tcb3
SMP
C2
TM
(D)
Rank 1
Rank 2
Rank 3
Rank 4
Rank 5
Tcb1
Tcb3
Tcb2
(E)
(i) Tcb1 Tcb2 Tcb3
(v) Tcb1 Tcb2 Tcb3(TM)
(vi) tcb1Δ tcb2Δ Tcb3(TM)
PM or Golgi
ER
Tcb1 Tcb3 Tcb2
Normal Vacuole morphology
Normal Vacuole morphology
Vacuole FRAGMENTATION

694

695 **Figure 2. Effects of domain deletion and artificial tether on vacuole morphology**
696 (A) Diagram of domain organization of Tcb3 protein. TM, transmembrane domain; SMP,
697 synaptotagmin-like mitochondrial lipid-binding protein; C2, calcium-dependent lipid-binding
698 domain; GBP, GFP-binding protein.
699 (B) Cells (FKY2577 (i), FKY2924 (ii), FKY3903 (iii), FKY3904 (iv), FKY3905 (v) and FKY4754 (vi))
700 were grown overnight at 25 ºC in YPD. Then vacuoles were stained with FM4-64 and imaged by
701 fluorescence microscopy. The number of vacuoles per cell was counted and categorized into one
702 of three groups. The data represent mean ± SE of three independent experiments, each based on
703 more than 100 cells. *$p < 0.05$ and **$p < 0.01$ by Student's t-test compared with Tcb1 Tcb2 Tcb3
704 (i). Significant differences analysis between the pairwise combination of groups was performed
705 using two-way ANOVA.
706 (C) The modeled structures of the Tcb1p, Tcb2p and Tcb3p proteins. The ribbons and arrows
707 indicate alpha-helices and beta-sheets, respectively.
708 (D) TM domain complex in Tcb1p (red), Tcb2p (green), and Tcb3p (blue). The rank "X" indicates
709 the order in which the complexes are most likely to form.
710 (E) Illustrations show that TM domain of Tcb3 contributes to mediating protein interactions between
711 the tricalbin family to maintain vacuolar morphology.
712

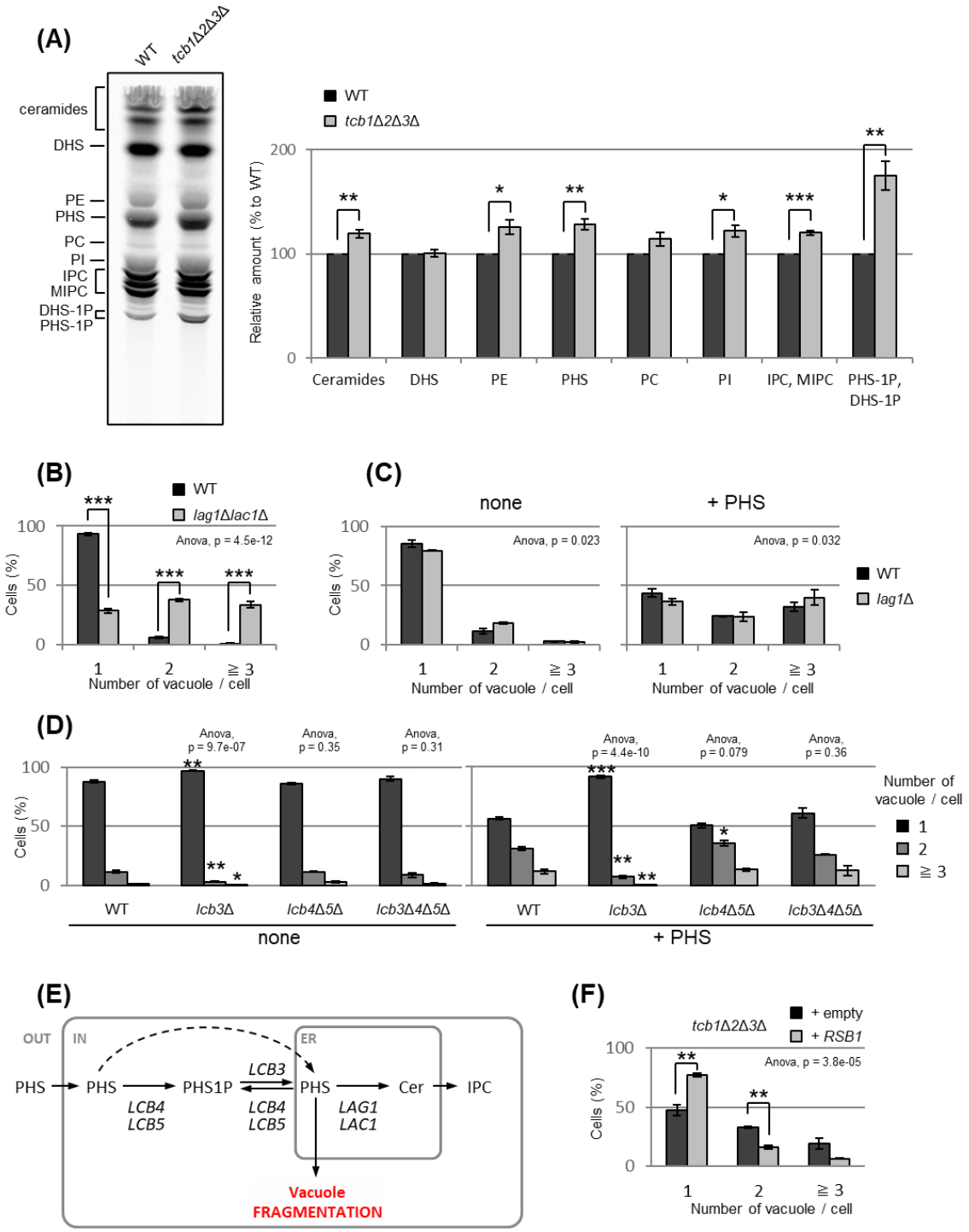

Figure 3. Accumulated PHS in *tcb1Δ2Δ3Δ* causes vacuole fragmentation.

(A) Cells (FKY2577 and FKY2927) were grown at 25˚C, and labeled with [^{3}H]DHS for 3 hours. Labelled lipids were applied to TLC plates using solvent system (Chloroform-methanol-4.2N ammonium hydroxide (9:7:2, v/v/v)). Incorporation of [^{3}H]DHS into each lipid was quantified and

718 the percentage of the total radioactivity (%) in WT cells was determined. Data represent mean ±
719 SE of four independent experiments. ** P < 0.01 by Student's t-test.
720 (B-D, F) Cells (FKY5687 and FKY5688 in B; FKY3340 and YKC121-59 in C; FKY36, FKY37,
721 FKY33 and FKY38 in D; FKY2927 in F) were grown overnight at 25 ºC in YPD. PHS was added at
722 160 μM (C) or 80 μM (D) for 2 hours. Vacuoles were stained with FM4-64 and imaged by
723 fluorescence microscopy. The number of vacuoles per cell was counted and categorized into one
724 of three groups. The data represent mean ± SE of three independent experiments, each based on
725 more than 100 cells. *p < 0.05, **p < 0.01 and ***p<0.001 by Student's t-test compared with WT
726 (B, D) or empty cells (F). Significant differences analysis between the pairwise combination of
727 groups was performed using two-way ANOVA.
728 (E) Illustration showing intracellular utilization pathway of exogenous PHS.
729

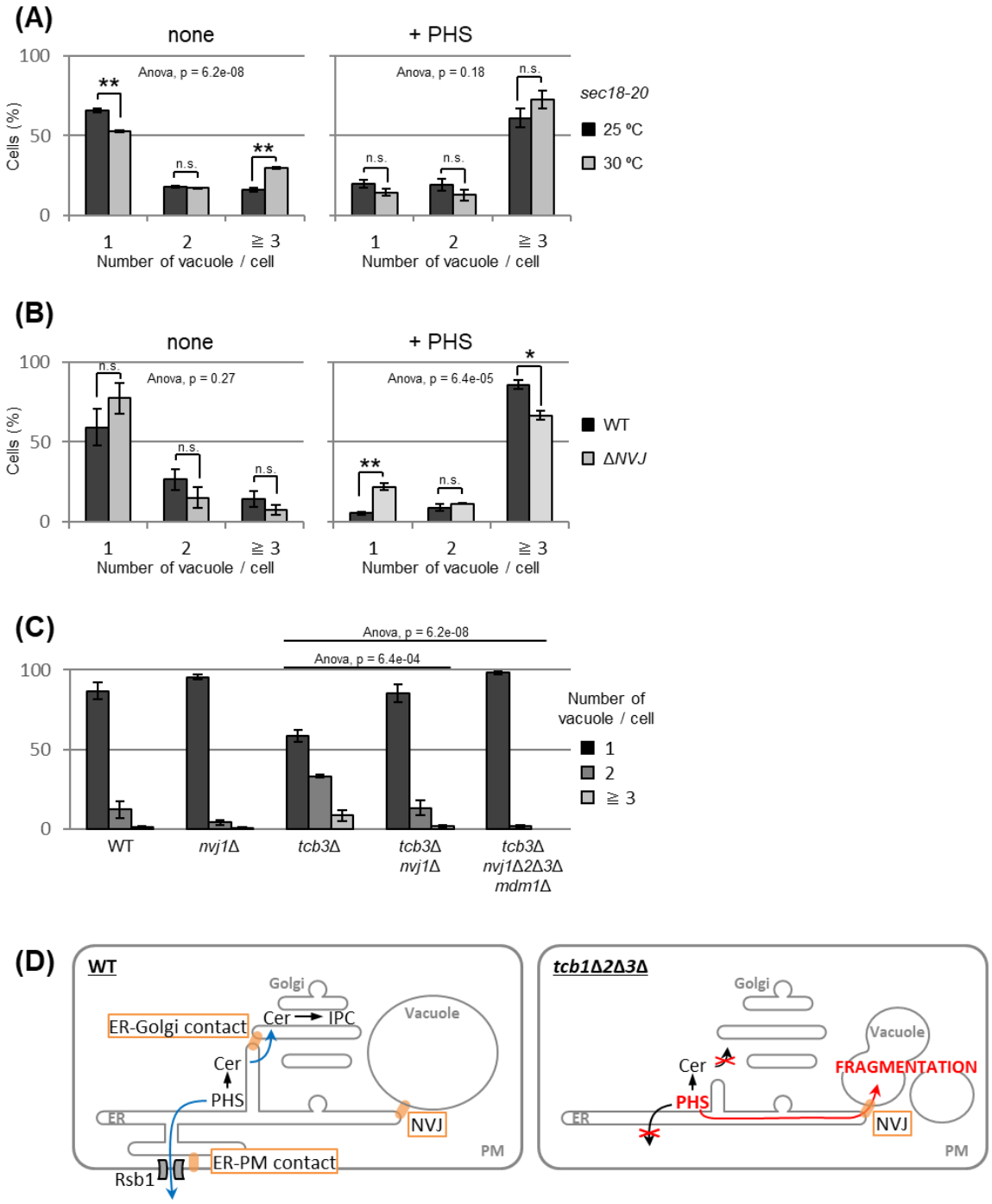

Figure 4. NVJ is required for PHS-induced vacuole fragmentation

(A-C) Cells (FKY2929 in A; FKY3868 and FKY5560 in B; FKY6187, FKY6189, FKY6190, FKY6188 and FKY6409 in C) were grown overnight at 25 ºC in YPD. PHS was added at 40 μM for 2 hours at 30 ºC (A) and 25 ºC (A, B). Vacuoles were stained with FM4-64 and imaged by fluorescence microscopy. The number of vacuoles per cell was counted and categorized into one of three

736 groups. The data represent mean ± SE of three independent experiments, each based on more
737 than 100 cells. *$p < 0.05$, **$p < 0.01$ and ***$p<0.001$ by Student's t-test. Significant differences
738 analysis between the pairwise combination of groups was performed using two-way ANOVA.
739 (D) Membrane contact sites regulate vacuole morphology via sphingolipid metabolism. See the
740 main text for details.
741

742 **Supplementary information**

743

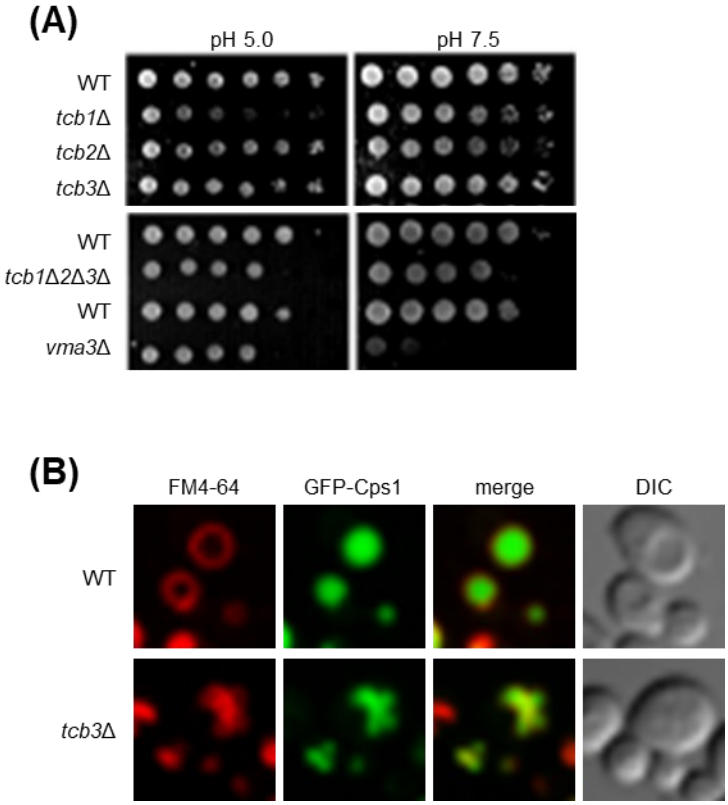

744

745 **Supplementary Figure 1**

746 (A) Cells (FKY2577, FKY2909, FKY3819, FKY2924, FKY2927, FKY3340 and YKC112-01) were
747 adjusted to OD_{600} = 1.0 and fivefold serial dilutions were then spotted on YPD plates of indicated
748 pH, then incubated at 25 ºC.

749 (B) GFP-Cps1p fusion protein was transformed into WT (FKY2577) and *tcb3*Δ (FKY2924) strains
750 and analyzed its subcellular localization with respect to FM4-64-stained vacuoles using by
751 fluorescent microscopy.

752

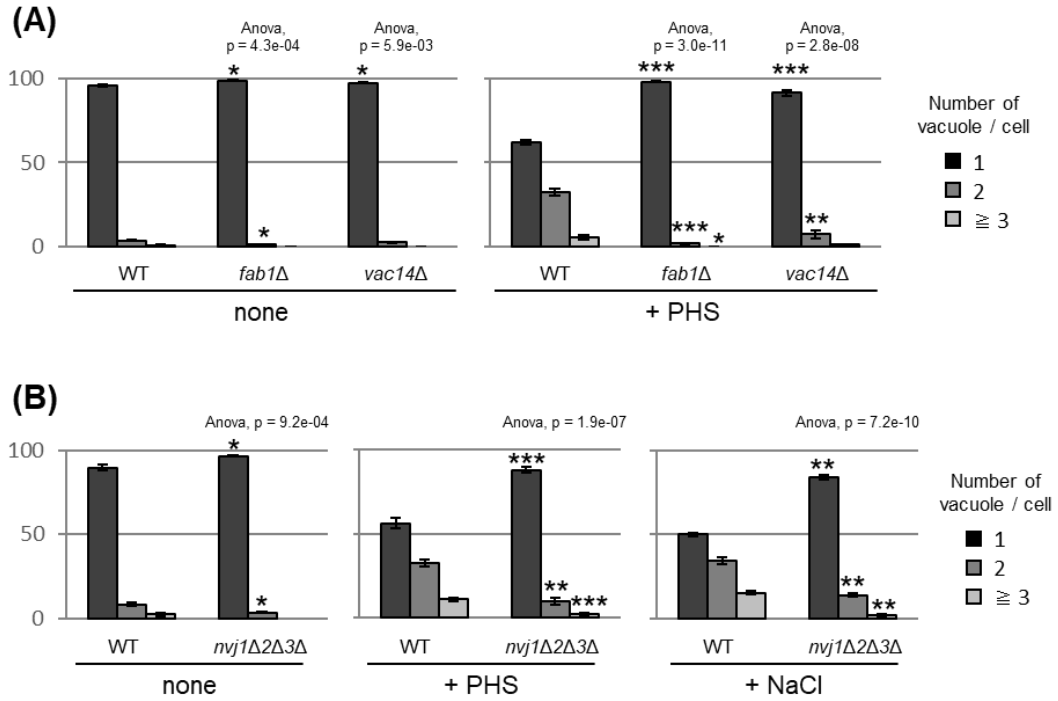

Supplementary Figure 2

(A, B) Cells (FKY3340, YKC145-21 and YKC149-61 in A; FKY6187 and FKY6140 in B) were grown overnight at 25 ºC in YPD. PHS was added at 80 μM for 2 hours, or cells were incubated with 0.2 M of NaCl for 2 hours. Vacuoles were stained with FM4-64 and imaged by fluorescence microscopy. The number of vacuoles per cell was counted and categorized into one of three groups. The data represent mean ± SE of three independent experiments, each based on more than 100 cells. *p < 0.05, **p < 0.01 and ***p<0.001 by Student's t-test. Significant differences analysis between the pairwise combination of groups was performed using two-way ANOVA.

763 **Supplementary Table 1**

764 Yeast strains used in this study, Related to All Figures.

Strain	Number	MAT	Genotype	Source
WT (RH)	FKY2577	a	*ura3 his3 leu2 trp1 lys2 bar1-1*	Ikeda A et al. iScience. 2020;23(10):101603.
*tcb1*Δ*2*Δ*3*Δ	FKY2927	a	RH except for *tcb1*Δ::*TRP1 tcb2*Δ::*HIS3 tcb3*Δ::*LEU2*	Ikeda A et al. iScience. 2020;23(10):101603.
*tcb1*Δ	FKY2909	a	RH except for *tcb1*Δ::*TRP1*	Ikeda A et al. iScience. 2020;23(10):101603.
*tcb2*Δ	FKY3819	alpha	RH except for *tcb2*Δ::*HIS3*	Ikeda A et al. iScience. 2020;23(10):101603.
*tcb3*Δ	FKY2924	a	RH except for *tcb3*Δ::*LEU2*	Ikeda A et al. iScience. 2020;23(10):101603.
*tcb1*Δ*2*Δ	FKY3023	a	RH except for *tcb1*Δ::*TRP1 tcb2*Δ::*HIS3*	Ikeda A et al. iScience. 2020;23(10):101603.
*tcb1*Δ*3*Δ	FKY3820	alpha	RH except for t*cb1*Δ::*TRP1 tcb3*Δ::*LEU2*	Ikeda A et al. iScience. 2020;23(10):101603.
*tcb2*Δ*3*Δ	FKY3008	a	RH except for *tcb2*Δ::*HIS3 tcb3*Δ::*LEU2*	Ikeda A et al. iScience. 2020;23(10):101603.
TCB3 (Full)-GBP	FKY3903	a	RH except for *TCB3-GBP*Δ::*KanMX*	This study
TCB3 (TM-SMP)-GBP	FKY3904	a	RH except for *TCB3* (1F-489R)-*GBP*::*KanMX*	This study
TCB3 (TM)-GBP	FKY3905	a	RH except for *TCB3* (1F-259R)-*GBP*::*KanMX*	This study
*tcb1*Δ*2*Δ *TCB3* (TM)-GBP	FKY4754	a	RH except for *tcb1*Δ::*TRP1 tcb2*Δ::*HIS3 TCB3* (1F-259R)::*KanMX*	This study
WT	FKY36 / RH4423	alpha	RH except for *HIS3* + *TRP1* + *LYS2* + *pep4-3*	Funato K et al. J Biol Chem. 2003;278(9):7325-7334.
*lcb3*Δ	FKY37 / RH4427	alpha	RH except for *lcb3*Δ::KanMX *HIS3* + *LEU2* + *TRP1* + *LYS2* + *pep4-3*	Funato K et al. J Biol Chem. 2003;278(9):7325-7334.
*lcb4*Δ*5*Δ	FKY33 / RH4402	alpha	RH except for *lcb4*Δ::*URA3 lcb5*Δ::*LEU2 HIS3* + *TRP1* + *LYS2* + *pep4-3*	Funato K et al. J Biol Chem. 2003;278(9):7325-7334.
*lcb3*Δ*4*Δ*5*Δ	FKY38 / RH4464	alpha	RH except for *lcb3*Δ::*kanMX lcb4*Δ::*URA3 lcb5*Δ::*LEU2 HIS3* + *TRP1* + *LYS2* + *pep4-3*	Funato K et al. J Biol Chem. 2003;278(9):7325-7334.
sec18-20	FKY2929	alpha	RH except for *sec18-20 LYS2*+	Ikeda A et al. iScience. 2020;23(10):101603.
WT (RH)	FKY6187	alpha	*ura3 his3 leu2 trp1 lys2 bar1-1*	This study
*nvj1*Δ	FKY6189	a	RH except for *nvj1*Δ::*HIS3*	This study
*tcb3*Δ	FKY6190	alpha	RH except for *tcb3*Δ::*LEU2*	This study
*tcb3*Δ*nvj1*Δ	FKY6188	a	RH except for tcb3Δ::*LEU2* nvj1Δ::HIS3	This study
*tcb3*Δ*nvj1*Δ*2*Δ*3*Δ*mdm1*Δ	FKY6409	a	RH except for *nvj1*Δ:: *URA3 nvj2*Δ::*KanMX nvj3*Δ::*HIS3 mdm1*Δ::*KanMX tcb3*Δ::*LEU2*	This study
nvj1Δ2Δ3Δ	FKY6140	a	RH except for nvj1Δ:: URA3 nvj2Δ::KanMX nvj3Δ::HIS3	This study
WT (W303)	FKY5687 / RL1	a	*his3-11,15 leu2-3,112 trp1-1 ura3-1 ade2-1 can1-100 GAL + bar-*	Lucena R et al. Curr Biol. 2018;28(2):196-210.
*lag1*Δ*lac1*Δ	FKY5688 / RL40	a	W303 except for *lag1*Δ::*KanMX6 lac1*Δ::*HIS*	Lucena R et al. Curr Biol. 2018;28(2):196-210.
WT (BY4742)	FKY3340	alpha	*his3*Δ*1 leu2*Δ*0 lys2*Δ*0 ura3*Δ*0*	Open biosystem, inc
*lag1*Δ	YKC121-59	alpha	BY4742 except for *lag1*Δ::*KanMx*	Open biosystem, inc
*vma3*Δ	YKC112-01	alpha	BY4742 except for *vma3*Δ::*KanMx*	Open biosystem, inc
*fab1*Δ	YKC145-21	alpha	BY4742 except for *fab1*Δ::*KanMx*	Open biosystem, inc
*vac14*Δ	YKC149-61	alpha	BY4742 except for *vac14*Δ::*KanMx*	Open biosystem, inc
WT (SEY6210)	FKY3868	alpha	*ura3-52 leu2-3,112 his3-Δ100 trp1-Δ901 lys2-801 suc2-Δ9*	Yabuki Y et al. Genetics. 2019;212(1):175-186.
Δ*NVJ*	FKY5560	alpha	SEY6210 except for *nvj1*Δ::*TRP1 nvj2*Δ::*HIS3 nvj3*Δ::*NatMX mdm1*Δ::*KanMX*	Henne WM et al. J Cell Biol. 2015;210(4):541-551.

765

766

767 **Supplementary Table 2**

768 Plasmids used in this study, Related to All Figures.

Plasmid	Number	Relevant information	Source
pRS426-TDH3	FKP51	2μ, yeast *TDH3* promoter, empty, *URA3*	Mumberg D et al., Gene. 1995;156(1):119-122
pRS426-TDH3/RSB1	FKP1065	2μ, yeast *TDH3* promoter, *RSB1* , *URA3*	This study
pRS316/PTDH3-EGFP-CPS1-TCMK1	FKP621	CEN, yeast *TDH3* promoter, GFP-*CPS1* *URA3*	Howard Riezman

769

770